The Cryosphere, 8, 1139–1148, 2014
www.the-cryosphere.net/8/1139/2014/
doi:10.5194/tc-8-1139-2014

The Cryosphere
Open Access

Measuring the specific surface area of wet snow using 1310 nm reflectance

J.-C. Gallet[1], **F. Domine**[2,3], **and M. Dumont**[4]

[1]Norwegian Polar Institute, Tromsø, Norway
[2]Takuvik Joint International Laboratory, Université Laval (Canada) and CNRS-INSU (France), Pavillon Alexandre Vachon, 1045 avenue de La Médecine, Québec, QC, G1V 0A6, Canada
[3]Department of Chemistry, Université Laval, Québec, QC, Canada
[4]Météo-France – CNRS, CNRM-GAME UMR3589, CEN, Grenoble, France

Correspondence to: F. Domine (florent.domine@gmail.com)

Received: 1 October 2013 – Published in The Cryosphere Discuss.: 31 October 2013
Revised: 2 May 2014 – Accepted: 16 May 2014 – Published: 3 July 2014

Abstract. The specific surface area (SSA) of snow can be used as an objective measurement of grain size and is therefore a central variable to describe snow physical properties such as albedo. Snow SSA can now be easily measured in the field using optical methods based on infrared reflectance. However, existing optical methods have only been validated for dry snow. Here we test the possibility to use the DUFISSS instrument, based on the measurement of the 1310 nm reflectance of snow with an integrating sphere, to measure the SSA of wet snow. We perform cold room experiments where we measure the SSA of a wet snow sample, freeze it and measure it again, to quantify the difference in reflectance between frozen and wet snow. We study snow samples in the SSA range 12–37 $m^2\ kg^{-1}$ and in the mass liquid water content (LWC) range 5–32 %. We conclude that the SSA of wet snow can be obtained from the measurement of its 1310 nm reflectance using three simple steps. In most cases, the SSA thus obtained is less than 10 % different from the value that would have been obtained if the sample had been considered dry, so that the three simple steps constitute a minor correction. We also run two optical models to interpret the results, but no model reproduces correctly the water–ice distribution in wet snow, so that their predictions of wet snow reflectance are imperfect. The correction on the determination of wet snow SSA using the DUFISSS instrument gives an overall uncertainty better than 11 %, even if the LWC is unknown. If SSA is expressed as a surface to volume ratio (e.g., in mm^{-1}), the uncertainty is then 13 % because of additional uncertainties in the determination of the volume of ice and water when the LWC is unknown.

1 Introduction

Snow is a porous medium made of air, ice, small amounts of impurities and occasionally liquid water. It is one of the most, or perhaps even the most reflective surface on earth so that its albedo is a key parameter to determine the planetary energy budget (Hall, 2004; Lemke et al., 2007). The albedo of snow is determined mostly by its impurity content and grain size, but the liquid water content (LWC) also plays a role (Warren, 1982). In the visible range of the solar spectrum, the albedo of dry snow is little dependent on the snow grain size and is mostly controlled by the impurity content. In the infrared, snow grain size controls the albedo of dry snow (Warren, 1982). The effect of water on snow albedo depends on its location. When present in small amounts, water is located only at grain boundaries (Colbeck, 1973; Ketcham and Hobbs, 1969) and a slight decrease in albedo is observed (Wiscombe and Warren, 1980). For a high water fraction, water entirely coats the snow grains so that large water–ice clusters are formed resulting in a larger decrease in albedo (Colbeck, 1973).

Even if the contrast between water and ice refractive indices is small, maxima and minima for water are shifted towards shorter wavelengths, as shown in Fig. 1 (Segelstein, 1981; Warren and Brandt, 2008; Kou et al., 1993) so that a

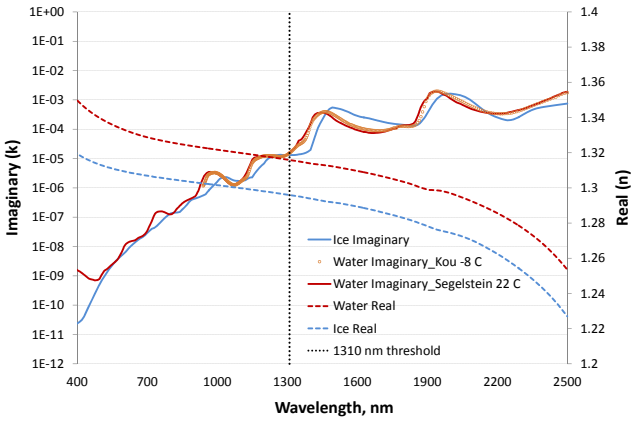

Figure 1. Real and imaginary indices of refraction of ice (from Warren et al., 2008) and water (from Segelstein, 1981 and Kou et al., 1993).

spectral signature is expected when sufficient amounts of water are present in the snowpack (Green et al., 2002), in particular in the 950–1150 nm range. Several investigations of the spectral signature of snow surfaces have been carried out in that wavelength range for remote sensing purposes, in order to retrieve the snow grain size and/or liquid water content (Dozier and Painter, 2004; Green et al., 2002, 2006; Nolin and Dozier, 2000). Nolin and Dozier (2000) concluded that the effect of liquid water is negligible in the 950–1150 nm range for the purpose of snow grain size retrieval if the LWC is lower than 5 % per volume. In that wavelength range, the spectral shift between ice and water is at its maximum, and differences in the imaginary part of the index of refraction reach a factor of 3. At 1310 nm, ice and water present close values of indices of refraction (1.5 and 17 % higher for water respectively for the real and the imaginary parts) so that the effect of water should be weak. The present work describes the possibility of retrieving the grain size of wet snow from the measurement of reflectance at 1310 nm.

Given the highly variable shapes of snow grains, the notion of "snow grain size" has long been not very well defined and varies from one study to another (Aoki et al., 2000). More recent studies have used the surface / volume ratio, i.e., the snow specific surface area (SSA), to determine the optical properties of the snow. The snow SSA is usually defined as the surface area per unit mass (Legagneux et al., 2002),

$$\mathrm{SSA} = \frac{S}{M} = \frac{S}{\rho_{\mathrm{ice}} \times V} = \frac{3}{\rho_{\mathrm{ice}} \times r_{\mathrm{eff}}}, \quad (1)$$

with S the surface area of snow grains, M their mass, V their volume, ρ_{ice} the density of ice (917 kg m^{-3} at 0 °C) and r_{eff} the effective radius of the snow grains, i.e., the radius of ice spheres having the same SSA as the snow. This radius is sometimes called the optical radius. For dry snow, the SSA quantifies the ice–air interface per unit mass. For wet snow, it quantifies the sum of the ice–air and water–air interfaces per unit mass. The snow SSA is a physical quantity that requires no assumption regarding grain shape and is expressed in m^2 kg^{-1} with measured values ranging from 1.9 to 223 m^2 kg^{-1} for dry snow (Domine et al., 2007, 2011).

In field studies, when wet snow is encountered, air temperature is often above 0 °C so that the sample cannot be refrozen on site. All current snow SSA measurement techniques have been developed and validated for dry snow. Many techniques, such as CH_4 adsorption (Domine et al., 2007) or X-ray tomography (Flin et al., 2004), cannot be used because they require that the snow be frozen. Optical methods, on the other hand, are potentially appropriate. Such methods have been used to measure the SSA of dry snow (Arnaud et al., 2011; Gallet et al., 2009; Matzl and Schneebeli, 2006; Montpetit et al., 2012; Painter et al., 2007; Picard et al., 2009), but none has been tested for wet snow. Here we used the DUFISSS instrument (Gallet et al., 2009) to measure the 1310 nm reflectance of wet snow. Briefly, Gallet et al. (2009) used an integrating sphere to measure the reflectance of a snow sample at 1310 or 1550 nm and determined its SSA with a calibration curve obtained by the simultaneous measurement of reflectance and SSA using CH_4 adsorption. The shorter wavelength was used for SSA lower than 60 m^2 kg^{-1} while the longer one was used for higher snow SSA. The estimated accuracy of this instrument is 10 % and allows a fast measure of SSA in the field for every type of dry snow.

To extend the validation of the method to wet snow, experiments were performed in a cold room. We used DUFISSS to measure the 1310 nm reflectance of wet snow of known density and liquid water content. We then let the wet snow sample refreeze and measured its reflectance again, so that the reflectances of the same snow sample, wet and frozen, could be compared. Radiative transfer calculations using the DISORT model (Stamnes et al., 1988) were also used in order to compare our cold room data set with theoretical calculations.

2 Experimental protocol

The idea of our cold room experiments was to prepare a homogeneous wet snow sample. We then measured its density and LWC and took a sample whose reflectance was measured at 1310 nm with DUFISSS placed in a cold room at −2.2 °C. The sample was then allowed to refreeze without any disturbance to its structure so that the reflectance of the very same sample could be measured again once refrozen. During freezing, several processes could take place that may result in structural changes that could affect SSA. These include (1) metamorphism and the related SSA decrease and (2) structural changes caused by the crystallization of water. Regarding (1), using the Crocus model (Brun et al., 1992), we calculated that the time to refreeze the first cm of our snow sample is of the order of 15 to 20 min, under the conditions in our cold room. Within this timescale, we calculate using Eq. (13) of Taillandier et al. (2007) that snow with an initial SSA of

$40\,m^2\,kg^{-1}$ would decrease to $39\,m^2\,kg^{-1}$ after an hour. For lower SSAs and lower durations, the SSA decrease would be even less and therefore hardly detectable. Regarding (2), the work of Brzoska et al. (1998) showed that snow subjected to flash freezing, a process much more prone to produce structural changes than the slow freezing used here, did not lead to any detectable structural change. Furthermore, scanning electromicrographs by Erbe et al. (2003) (their Fig. 9) and Wergin et al. (1995) (their Fig. 17) show that refreezing of melted snow did not produce any detectable structural changes, as what was observed was just the solidification of the liquid water, without the formation of any other structure that could perturb SSA. Based on these considerations, we conclude that frozen snow most likely has a structure and a SSA comparable to that of the parent wet sample, except for effects due to volume expansion.

The snow used was taken from large plastic boxes filled with snow from the mountains around Grenoble and stored at $-20\,°C$. Snow from two distinct snowfalls was used: one about a week old and the other from the previous season. To make uniform samples, batches of about 500 g of snow were mixed in a dough kneader placed in a cold room at $-2.2\,°C$. Several such batches were placed inside a large plastic box and were further mixed with a shovel. The resulting sample was then transferred into a Plexiglas box $15\,cm \times 25\,cm$ in horizontal section and 25 cm in height.

To obtain a wet snow sample, we used the method detailed by Brun (1989). Briefly, the Plexiglas box was placed between two conductor plates within an insulated box, and between these plates a current of 4000 V at 20 kHz was applied. The instrument was also located in the cold room at $-2.2\,°C$. At 20 kHz frequency, the energy absorption by snow is such that homogeneous heating is produced, so that a uniform LWC content can be obtained. Of course, the LWC is not perfectly uniform because of conductive losses at the edges. Furthermore, percolation can take place if the LWC exceeds the percolation threshold (Coleou and Lesaffre, 1998). However, the results showed that possible moderate variations in LWC within the box are not critical.

Six snow samples were heated for durations between 23 and 90 minutes. The Plexiglas box was then taken out of the heater and placed on a bench in the cold room at $2.2\,°C$. Snow density was then measured using a $100\,cm^3$ tubular cutter that was weighted, showing densities between 153 and $296\,kg\,m^{-3}$. The LWC was determined using the apparatus described in Brun (1989). Briefly, the relative permittivity of the snow was measured in a cylindrical capacitor of $330\,cm^3$ at a frequency around 18 mHz. LWCs between 5 and 32 % in mass were obtained.

Two snow samples were then taken for IR reflectance measurements at 1310 nm using the exact protocol detailed in Gallet et al. (2009). Briefly, a cylindrical snow core 63 mm in diameter and 30 mm high was placed in a 25 mm high cylindrical container. The extra 5 mm were then shaved off with a metal spatula. Ideally, the spatula should be exactly at $0\,°C$ so that no freezing or melting occurs. Initially the spatula was at $-2.2\,°C$ in the cold room. After trial and error, holding the spatula between both gloved hands for 3 s appeared to minimize disturbance to the sample structure, in that neither glazing from a too cold spatula nor the appearance of extra liquid water was observed. In any case, the penetration depth (i.e., the depth were the light flux is divided by e) of the 1310 nm radiation in the snow types studied was about 1 cm (Gallet et al., 2009), so that minimal surface perturbation due to our protocol had little influence on measured reflectance. The snow sample was then allowed to freeze. A total of 12 samples were thus measured, two for each experiment. Since density, LWC and reflectance required distinct samples, and since given the amount of snow available only one density and one LWC measurement were done, the density and LWC values found were ascribed to both snow samples whose reflectance were measured, even though there were certainly slight variations within the Plexiglas box. The SSA was computed from reflectance using a polynomial fit of the SSA–reflectance relationship as described in Gallet et al. (2009). Here, we use the same relationship for wet and dry snow, although it only holds for dry snow and the value obtained for wet snow is therefore only an apparent SSA (SSA_{app} hereafter), from which we subsequently try to extract the actual wet snow SSA.

A possible issue is that, since snow crystal shape may affect reflectance (Picard et al., 2009), the dry snow algorithm, which approximates snow crystals as spheres, may not hold for wet snow. When snow is melting, edges are rounded off and grains become more spherical (Colbeck, 1982), so that wet snow shapes are closest to those used in the model, which is therefore expected to perform even better than for dry snow.

3 Model description

The modeling study is the same as that used by Green et al. (2002). It is based on the Discrete-ORdinate Radiative Transfer code (DISORT) (Stamnes et al., 1988). DISORT calculates the reflectance of a succession of horizontally infinite plane-parallel snow layers under direct and/or diffuse illumination knowing the optical properties of each layer. The required input properties – namely the single scattering albedo, the extinction efficiency and the phase function – are calculated using either of the following two codes: Mie (Wiscombe and Warren, 1980) or the layered-sphere Mie calculations (Toon and Ackerman, 1981). The differences between both models are therefore only due to the use of either Mie or the layered code.

Mie calculations were used for spherical ice grains and liquid water spheres. This results in droplets of water being present in the interstitial space between ice grains. Optical properties were calculated for both materials and mixed by weighted average (Warren and Wiscombe, 1980). The second

Table 1. Density, liquid water content (LWC), reflectance at 1310 nm (R), and specific surface area (SSA $m^2\ kg^{-1}$) of the samples studied, wet at 0 °C and frozen. SSAs for wet samples are apparent values as defined in the text.

Snow sample name	Heating time, min	Density Wet snow $kg\ m^{-3}$	LWC, mass %	*R* wet snow	*R* frozen snow	SSA_{app} wet snow	SSA frozen snow	*R* frozen – *R* wet	SSA frozen – SSA_{app} wet	SSA frozen – SSA_{app}, %
cen_1	45	182	9.6	0.4411	0.4437	35.5	35.6	0.0030	0.10	0.3
cen_2	45	182	9.6	0.4321	0.4326	33.4	33.5	0.0005	0.10	0.3
cen_3	86	283	31.0	0.3215	0.3215	18.4	18.4	0.00	0.00	0.0
cen_4	86	283	31.0	0.2435	0.2509	12.1	12.6	0.0074	0.50	4.0
cen_5	23	208	5.0	0.4399	0.4439	34.9	35.6	0.0040	0.70	2.0
cen_6	23	208	5.0	0.4503	0.4541	36.9	37.7	0.0038	0.80	2.1
cen_7	90	296	32.1	0.2936	0.3014	15.9	16.5	0.0078	0.60	3.6
cen_8	90	296	32.1	0.4321	0.4570	33.4	38.2	0.0249	4.80	12.6
cen_9	43	153	7.2	0.4301	0.4298	33.0	33.0	−0.0003	0.00	0.0
cen_10	43	153	7.2	0.4480	0.4512	36.4	37.1	0.0032	0.70	1.9
cen_11	60	260	21.6	0.3082	0.3155	17.1	17.8	0.0073	0.70	3.9
cen_12	60	260	21.6	0.3180	0.3275	18.0	19.0	0.0090	1.00	5.3

approach is the layered calculation that represents snow as spheres made of a core of ice and a shell of water. In both cases, we have to deal with water and ice that have different densities, and we have to keep the SSA and mass constant for comparison. According to Eq. (1), if the SSA is $30\ m^2\ kg^{-1}$, it means that snow is made up of ice spheres of 109 µm radius while a pure water medium will be made of spheres of 100 µm radius. We therefore take this issue into account for both codes. Increasing the LWC in the Mie code will just replace ice spheres by water spheres with a radius lowered according to the ice–water densities ratio. Increasing the LWC in the layered code will decrease the radius of the outer sphere (core + shell), decrease the radius of the core made of ice and increase the thickness of the shell made of water. Figure 1 shows two sets of values for the imaginary part of the refractive index of water: one at 22 °C (Segelstein, 1981) and one for supercooled water at −8 °C (Kou et al., 1993). The −8 °C data set shows that the maxima and minima shifts of water are slightly less pronounced between 950 and 1150 nm than the 22 °C data set. As water in wet snow is around 0 °C, we will use the data set of (Kou et al., 1993).

For simplicity, we will use the term reflectance as equivalent to albedo, even though the proper term for our calculations and measurements is directional–hemispherical reflectance (Schaepman-Strub et al., 2006). To illustrate model performance and consistency, Fig. 2 presents the reflectance calculated with both codes for pure ice and pure water spheres for a SSA of $30\ m^2\ kg^{-1}$. All calculations have been done under direct illumination with a zero zenith angle and for an optically semi-infinite layer. As expected, the minima and maxima are shifted towards shorter wavelengths for water. Both codes show similar results for each medium with an average difference over the 800–1400 nm range lower than 0.3 % and 1.0 % for ice and water respectively.

Figure 3 shows calculations at 1310 nm (wavelength used in subsequent experiments) for snow SSAs of 5 and $30\ m^2\ kg^{-1}$ and LWC from 0 to 100 % per mass. At that

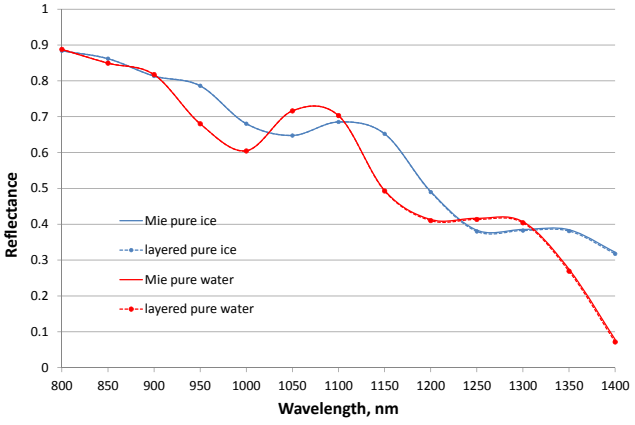

Figure 2. Reflectance calculated with both codes for snow of SSA = $30\ m^2\ kg^{-1}$ (pure ice and pure water), density = $300\ kg\ m^{-3}$ and an optically semi-infinite layer.

wavelength ice and water have very close refractive indices, with water absorbing and scattering slightly more. Mie shows reflectance values decreasing with increasing LWC because water absorbs more and because here, when the LWC increases, ice is replaced by water. For the layered code, the reflectance first increases and then decreases as LWC increases. Our understanding is that a small amount of water is creating a thin layer of water around the ice particles. Scattering is then enhanced while the increase in absorption is negligible for low LWC, explaining the increase in reflectance. For higher LWCs, the water shell is thicker and absorption is not negligible anymore so that reflectance decreases. The decrease in reflectance is observed slightly before for smaller SSA because the shell of water is thicker for the same amount of water compared to higher SSA. Average differences between the two codes are of 0.9 and 2.1 % respectively for SSAs of 30 and $5\ m^2\ kg^{-1}$ with maximum differences of

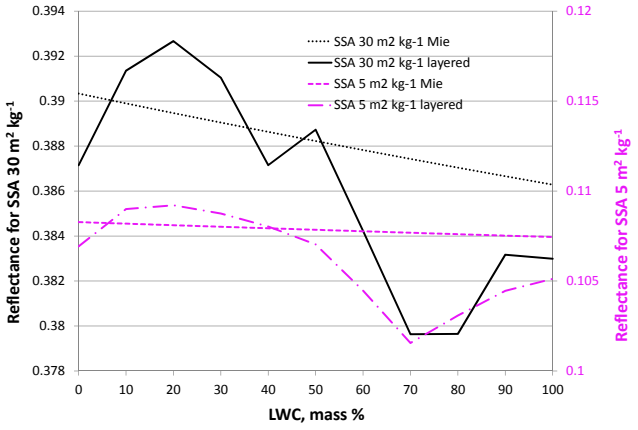

Figure 3. Effect of the LWC on the reflectance of snow for SSAs of 5 and 30 $m^2\,kg^{-1}$, density of 300 $kg\,m^{-3}$ and an optically semi-infinite layer at 1310 nm. Each SSA has its own vertical axis.

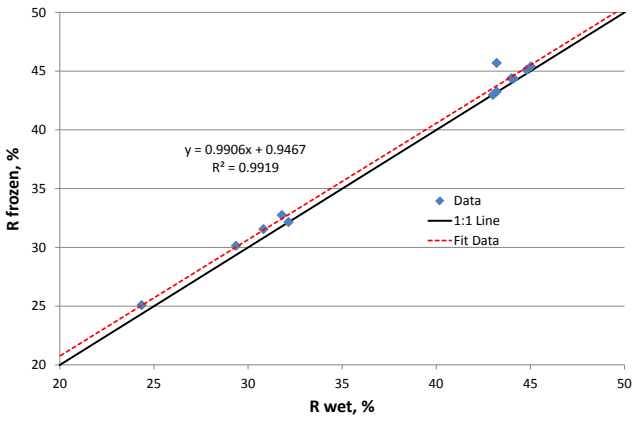

Figure 4. Correlation between the reflectances of the wet and frozen samples.

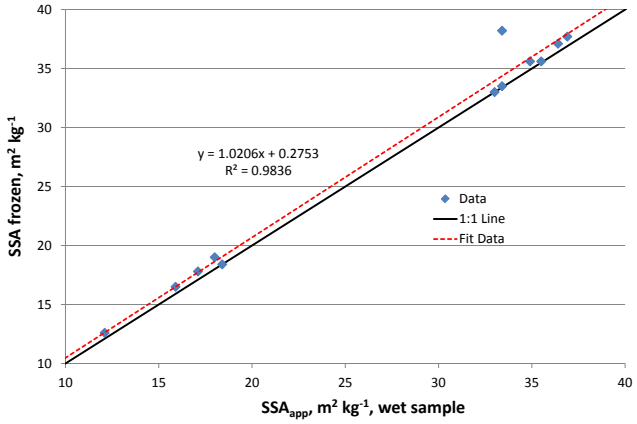

Figure 5. Correlation between the SSAs of the frozen samples, SSA_{frozen}, and the apparent SSA of the wet samples, SSA_{app}. SSA_{app} was determined from reflectance using the algorithm developed for dry snow.

5.7 % for 70 % LWC and low SSA. For reasonable values of LWC, i.e. below 40 %, the difference is no higher than 1.2 %.

However, neither Mie nor the layered codes represent correctly the location of water in the snowpack for low LWC. Ketcham and Hobbs (1969) showed that, in melting snow, water first appears as a meniscus on the ice surface where three grains join. Wet snow therefore obviously has water–ice interfaces, but the water coverage on ice is partial and of variable thickness. For higher LWC, water forms a continuous network (Colbeck, 1973) and even covers all the ice surfaces at sufficiently high LWC, so that the layered code may then be a reasonable approximation of processes, even though the thickness of the water film is never uniform. In any case, we test both codes over a wide LWC range below.

4 Results and discussion

The experimental results obtained are shown in Table 1, where the calculated SSAs for wet samples are apparent values. For four out of the six experiments, both samples from each experiment produced similar data, supporting our claim that our system produces fairly homogeneous snow. However, this does not seem to be valid for both samples with the highest LWC (31 and 32.1 mass %). These values certainly exceed the percolation threshold (Coleou and Lesaffre, 1998), resulting in large spatial variations and rapid changes in LWC, so that the values given are just indicative.

Figure 4 compares the reflectances of the wet and frozen samples. The differences are small. The sample cen_8 is an outlier. Figure 5 shows a similar graph for SSA and compares the SSA of the frozen sample, SSA_{frozen}, to the apparent SSA of the wet sample, SSA_{app}, which we retrieved using the relation from dry snow from Gallet et al. (2009). The outlier of Fig. 4 expectedly also shows up in Fig. 5. The maximum relative difference in reflectance is 3 %, corresponding to a SSA difference of 1 $m^2\,kg^{-1}$, if the outlier is not considered. We also calculated the difference in SSA, SSA_{frozen}–SSA_{app}, and plotted these as a function of LWC in Fig. 6. The correlation between SSA differences and LWC is low with $R^2 = 0.14$ (dashed red line). If the outlier is removed, R^2 values drop to 0.0001 (black solid line). These results show that the difference in SSA is not correlated to the LWC in the range studied. The mean SSA difference shown in Fig. 6 between frozen and wet samples is 0.5 $m^2\,kg^{-1}$ when the outlier is not considered.

We will then propose a simple modification of the algorithm used for dry snow to measure the SSA of wet snow in the field. What we measure is the reflectance of wet snow, R_{wet}, from which we deduced an apparent SSA, SSA_{app}, from the relationships f of Gallet et al. (2009):

$$SSA_{app} = f(R_{wet}). \quad (2)$$

From Fig. 6, we have determined experimentally that

$$\mathrm{SSA_{app}} = \mathrm{SSA_{frozen}} - 0.5\,\mathrm{m^2\,kg^{-1}}. \quad (3)$$

If we now assume that, upon freezing, no structural changes take place except those due to the volume expansion, we then have the actual SSA of the wet snow that verifies

$$\mathrm{SSA_{wet}} = \psi\,\mathrm{SSA_{frozen}}, \quad (4)$$

where ψ is a non intuitive factor that depends on the geometry of the snow and on the distribution of the water in the snow sample. Combining the above 3 equations, we obtain

$$\mathrm{SSA_{wet}} = (f(R_{\mathrm{wet}}) + 0.5)\,\psi. \quad (5)$$

The general form of ψ can be expressed as a function of the various interfaces in wet and frozen snow. We call $S_{\mathrm{a/i}}$ and $S_{\mathrm{a/w}}$ the area of the air–ice and air–water interfaces in wet snow and $S_{\mathrm{a/f}}$ the area of the interface between the air and the refrozen water in the frozen snow. Equation (4) then becomes

$$\mathrm{SSA_{wet}} = \mathrm{SSA_{frozen}}\frac{S_{\mathrm{a/i}} + S_{\mathrm{a/w}}}{S_{\mathrm{a/i}} + S_{\mathrm{a/f}}}. \quad (6)$$

Because of the expansion upon freezing, $S_{\mathrm{a/w}} < S_{\mathrm{a/f}}$ and ψ is therefore always less than 1 considering there are no other structural changes. If we make the approximation that wet snow consists of disconnected ice spheres surrounded by a homogenous water layer whose thickness is determined by the LWC, the ice in the wet snow is not in contact with the air so that we then have

$$\mathrm{SSA_{wet}} = \mathrm{SSA_{frozen}}\frac{S_{\mathrm{a/w}}}{S_{\mathrm{a/f}}}. \quad (7)$$

Also using Eqs. (4) and (5), we calculate that in this case we have

$$\mathrm{SSA_{wet}} = \quad (8)$$

$$(f(R_{\mathrm{wet}}) + 0.5)\left[1 - \mathrm{LWC}\left(1 - {}^{\rho_{\mathrm{ice}}}\!/_{\rho_{\mathrm{water}}}\right)\right]^{2/3},$$

with the derivation detailed in Appendix A. This expression is only an approximation based on a structural simplification, and we attempt to evaluate it in the subsequent modeling part. Assuming for the moment that this approximation is acceptable, we propose that to measure the SSA of wet snow with DUFISSS, we just need to measure its 1310 nm reflectance, obtain an apparent value from the relationships of Gallet et al. (2009), add $0.5\,\mathrm{m^2\,kg^{-1}}$ to that value, and then multiply by the factor ψ, which can be calculated with the coated sphere structural approximation (Eq. 8). We note that in general both these additive and multiplicative corrections are small and in opposite directions, so that in most cases corrections are minimal. This is illustrated in Fig. 7.

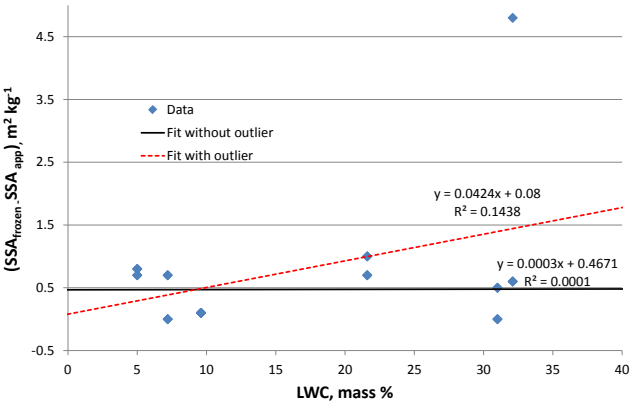

Figure 6. Difference between the SSA of the frozen sample and the apparent SSA of the wet sample ($\mathrm{SSA_{frozen}} - \mathrm{SSA_{app}}$) as a function of LWC.

ψ has a small effect and is between 0.9994 and 0.9778 respectively for LWC of 1 and 40 % per mass so that omitting ψ results in an uncertainty of < 2.2 %. The total correction is large only for very small SSAs, because the addition of $0.5\,\mathrm{m^2\,kg^{-1}}$ is not negligible in front of a low SSA value. For $\mathrm{SSA} \geq 5\,\mathrm{m^2\,kg^{-1}}$, the total correction is < 10 %, and for $\mathrm{SSA} \geq 10\,\mathrm{m^2\,kg^{-1}}$, the total correction is < 5 %. The data used to generate Fig. 7 show that not knowing the LWC results in uncertainties always less than 3 %, for LWC$<$ 0.40 and based on our disconnected coated spheres structural approximation. This deduction is in line with our experimental observation of Fig. 6 that LWC has a very limited impact on the correction.

In practice, omitting these corrections often results in deviations much smaller than the instrumental uncertainty, estimated at 10 % for dry snow (Gallet et al., 2009). The uncertainty in determining SSA of wet snow can be estimated from Eq. (8). Relative to the determination of the SSA of dry snow, extra uncertainties are due to the addition of (i) the $0.5\,\mathrm{m^2\,kg^{-1}}$ factor and (ii) the use of the ψ factor. To these, we must add (iii) uncertainties caused by our structural model approximation, used to derive Eq. (8). Given the strength of the $0.5\,\mathrm{m^2\,kg^{-1}}$ factor, uncertainty (i) is certainly negligible. Given the small impact of ψ, the resulting uncertainty can only be small, and in any case we estimate that (ii) causes an uncertainty < 1 %. The uncertainty caused by our structural model approximation is difficult to evaluate accurately. However, given that this model predicts a small effect of LWC on the correction while data indicate no effect, it is likely that the model introduces an uncertainty.

To explore this uncertainty in more detail, we estimated as a first step the effect of the LWC on the SSA using the Mie and layered codes. We ran both models using the geometry of our DUFISSS instrument as we did earlier (Gallet et al., 2009). This means that the snow is subjected to mostly direct lighting as well as to diffuse light due to the laser diode beam being reflected in the integrating sphere and

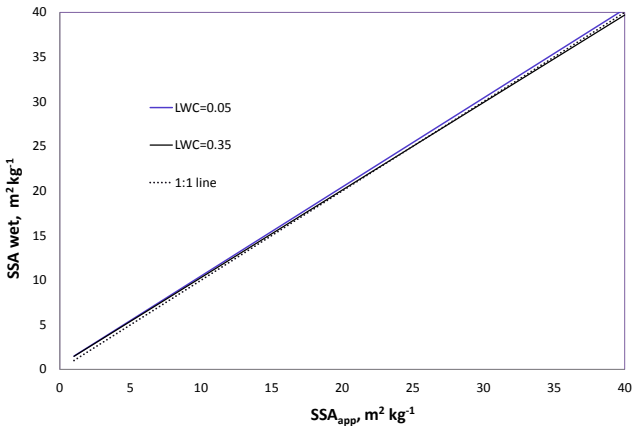

Figure 7. Relationship between the apparent SSA of a wet snow sample determined with DUFISSS using dry fit and that of the same sample whose SSA has been corrected according to Eq. (8), which takes into account reflectance and expansion effects. Calculations have been done for two realistic LWCs of snow.

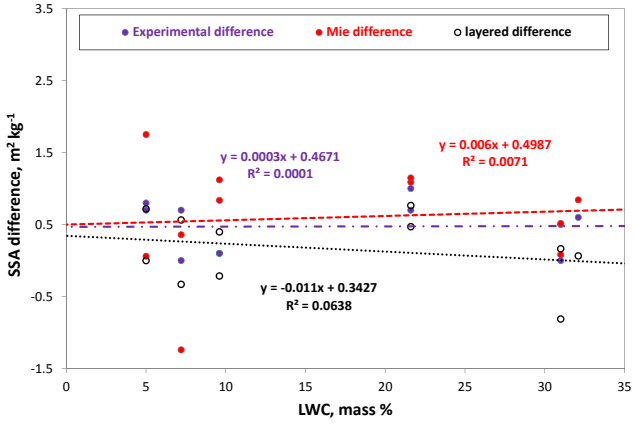

Figure 8. SSA differences between frozen and wet samples from measurements (purple) and estimated with models calculations with Mie (red) and the layered code (black).

re-illuminating the sample. We first calculated the reflectance of snow that should be measured by DUFISSS for samples having the properties of our experimental snow. Calculations were performed for dry and for wet snow with the LWCs determined experimentally. Both Mie and layered codes were used. The calculated reflectances were then converted into snow SSA using polynomial fits (Gallet et al., 2009). Slight modifications to the code had to be made, compared to Gallet et al. (2009) because of constraints in the layered code, as detailed in Appendix B.

These calculations yield the apparent SSA of wet snow, as determined in our experiments. Similarly to Fig. 6, we can plot the difference between the SSA of the frozen sample and the apparent SSA of the wet sample. This was done in Fig. 8, where data obtained using both models were plotted together with the experimental data. The outlier identified previously has been omitted. Figure 8 shows that the dry–wet differences are not the same for both codes and for the experimental data. This is expected since neither code reproduces the configuration of the actual sample, with respect to liquid water distribution. However, it is interesting to note that both codes show little correlation between the SSA difference and LWC, with correlation coefficients of only 0.007 and 0.06. This comforts our experimental result that the SSA difference does not depend on LWC and indicates that the difference depends mostly on the location of water. As water is simulated in Mie as single disconnected droplets and in the layered code as shells of water surrounding ice particles, both models simulate the two extreme cases where water could be located in a wet snow sample. In the Mie code, none of the ice surface is covered by water while all the ice is covered by water in the layered code. In natural samples, part or all of the ice is covered by water (Ketcham and Hobbs, 1969; Colbeck, 1973), depending on LWC. Figure 8 shows that the $0.5\,m^2\,kg^{-1}$ experimental difference is in between the values calculated by the models and both modelled SSA differences show a very weak (and in opposite direction) dependence to LWC so that neither of these codes can be discriminated. Since the physical representation of water by the layered code is much closer to reality as water is expected to cover all or most of the ice surfaces particularly for high LWC (Colbeck, 1973), we feel that the coated structural approximation used to derive Eq. (8) is adequate but not ideal to represent water in a wet snowpack, comforting its partial validity.

To estimate the uncertainty introduced by the use of the coated sphere approximation to derive Eq. (8), we investigated the differences between the experimental frozen SSA and the calculated wet snow SSAs but in a way slightly different from that presented in Fig. 8. Here, we used the measured LWC and wet reflectances to calculate the SSA of the wet snow samples using both models. We also used Eq. 8 introduced above. These three data sets (Mie, layered code and Eq. 8) yielding values of the SSA of wet snow are compared to the frozen SSA measured experimentally. The average differences between the experimental frozen SSA and the new calculated wet SSA are 1.9 %, 1.3 % and 2.9 %, for the Mie code, the layered code and the use of Eq. (8), respectively. The highest difference between the experimental frozen SSA and the calculated wet SSA is obtained using Eq. 8, with a value 1 % and 1.6 % higher than the Mie and the layered code, respectively. Thus, the uncertainty introduced by the use of the coated sphere approximation to derive Eq. (8) is estimated to be no higher than 2 %.

Since all the uncertainties envisaged are independent, the overall uncertainty is the square root of the sum of the squares of each error (10 % for DUFISSS, 1 % due to the ψ factor, 2 % for the coated sphere approximation), so that the overall uncertainty is 10.2 % for realistic values of LWC and for snow SSAs in the range 1–40 $m^2\,kg^{-1}$. If the LWC is unknown, an extra 3 % uncertainty, independent of the others,

has to be added, leading to a total 10.7 % uncertainty. The upper SSA limit of $40\,m^2\,kg^{-1}$ corresponds to our experiments and calculations, but there is no reason why the uncertainty would be higher for higher SSAs. Moreover, wet snow is unlikely to have high SSA values (Domine et al., 2007). The lower limit of $1\,m^2\,kg^{-1}$ corresponds to our calculations. Lower values must be rare, as the lowest value measured so far is $1.9\,m^2\,kg^{-1}$ (Domine et al., 2007). We therefore estimate that the overall uncertainty of SSA measurement of wet snow using DUFISSS is at the most 11 %, if the LWC is not known.

Finally, SSA can also be defined as the surface area per unit volume of ice or water, rather than per unit mass of snow (Fierz et al., 2009). It is then conveniently expressed in mm^{-1}. This volumetric definition can be correlated to the mass definition presented in this work when snow is dry using the ice density ρ_{ice}:

$$SSA_{vol} = SSA_{mass} \times \rho_{ice}, \quad (9)$$

with SSA_{vol} and SSA_{mass} the volumetric and the mass definition, respectively. When snow is wet, we need to take into account the LWC-dependent density of the medium as it is made up of water and ice. Considering reasonable LWC values, the density of the medium will vary between 0.917 and 0.9502 for 0 and 40 % LWC per mass, respectively. If the LWC is not known, this will introduce an extra 4 % uncertainty in the estimation of SSA_{vol}. This is not independent of the 3 % uncertainty associated with not knowing the LWC mentioned above, so that in the case of the volume definition, the uncertainty resulting from not knowing the LWC is 7 %, bringing the overall uncertainty to 13 %, slightly higher than if the mass definition were used.

5 Conclusion

Gallet et al. (2009) showed that the DUFISSS instrument could measure reliably the SSA of every type of dry snow tested and in the field. Here, we show that DUFISSS can also measure the SSA of wet snow with an uncertainty of 11 %. Experimental data and modeling work have shown that the effect of the presence of water on snow reflectance at 1310 nm is weak and depends very little on snow SSA and LWC. Furthermore, in most cases, deriving the SSA of wet snow assuming that its reflectance–SSA relationship is similar to that of dry snow leads to small errors. For an accurate determination of the SSA of wet snow, however, we recommend to correct the SSA value determined using the experimental dry fit of Gallet et al. (2009) by adding $0.5\,m^2\,kg^{-1}$ and multiplying the value obtained by a factor close to 1, detailed in Eq. (8). Since the correction depends little on the LWC, not knowing the LWC is not critical and assuming a LWC of 10 % (i.e, a corrective factor $\psi = 0.994$) will result in errors < 2 %. Our experimental SSA ranged from 16 to $38\,m^2\,kg^{-1}$ with LWC from 5 to 32 %. Admittedly, one weakness of this study is that it did not measure snow with very low SSAs. However, given the linear character of Figs. 4 and 5, we feel that the resulting error caused by extrapolating our conclusion to low SSAs is most likely very small, and in any case smaller than the intrinsic measurement error of the IR reflectance method used, which is 10 % (Gallet et al., 2009).

Appendix A

This appendix details calculations to obtain Eq. (8), based on the structural approximation that wet snow consists of disconnected ice spheres with a shell of water. We need to express the factor ψ, i.e., the ratio $\frac{S_{a/w}}{S_{a/f}} = \left(\frac{r_w}{r_f}\right)^2$, with r_w the radius of the shell of water of r_i the radius of the core of ice, subscript w is for water, i for ice, a for air and f for the refrozen water.

$V_W = \frac{4}{3}\pi\left(r_w^3 - r_i^3\right)$ is the volume of water in the wet snow sample, and $V_f = \frac{4}{3}\pi\left(r_f^3 - r_i^3\right)$ is the volume of refrozen snow, with r_f the radius of the refrozen shell of water. The definition of the LWC gives us

$V_w = V_i \times \frac{\rho_i}{\rho_w} \times \frac{1-LWC}{LWC}$. Using the other equation of V_w above, we have

$$r_w^3 = r_i^3\left[\frac{\rho_i}{\rho_w}\left(\frac{LWC}{1-LWC}\right)+1\right]. \quad (A1)$$

Because the mass is constant, we have $V_w\rho_w = V_f\rho_f$. Using equation of V_w and V_f above and Eq. (A1), we can write $\frac{4}{3}\pi \times \left[r_i^3\left[\frac{\rho_i}{\rho_w}\left(\frac{LWC}{1-LWC}\right)+1\right] - r_i^3\right] \times \rho_w = \frac{4}{3}\pi\left(r_f^3 - r_i^3\right) \times \rho_f$, with $\rho_f = \rho_i$, so that

$$r_f^3 = r_i^3\left(\frac{1}{1-LWC}\right). \quad (A2)$$

Using Eqs. (A1) and (A2), $\left(\frac{r_w}{r_f}\right)^3 = 1 - LWC\left(1 - \frac{\rho_i}{\rho_w}\right)$ meaning that $\left(\frac{r_w}{r_f}\right)^2 = \left(1 - LWC\left(1 - \frac{\rho_i}{\rho_w}\right)\right)^{\frac{2}{3}}$. Therefore,

$$SSA_w = SSA_f\frac{S_{a/w}}{S_{a/f}} = SSA_f \times \left(1 - LWC\left(1 - \frac{\rho_i}{\rho_w}\right)\right)^{\frac{2}{3}}$$

$$= (f\,(R_{wet} + 0.5)) \times \left(1 - LWC\left(1 - \frac{\rho_i}{\rho_w}\right)\right)^{\frac{2}{3}}.$$

Appendix B

The calculations done for Fig. 8 follow the DUFISSS configuration detailed in Gallet et al. (2009). Both the Mie and layered codes used calculate the reflectance of a 25 mm thick snow sample. Direct nadir lighting is used, and diffuse lighting due to the light reflected by the sample onto the integrating sphere walls is taken into account. A collimation factor of 0.95 for the 1310 nm laser diode is used. The reflectances of both wet and frozen samples are calculated using both codes.

To obtain SSA from reflectance, a polynomial fit is used (Gallet et al., 2009). However, here the polynomial fit had to be recalculated to account for our different calculation conditions. In Gallet et al. (2009), a lognormal distribution of snow grain sizes was used. This could not be used in the layered code because that model splits the spheres that represent the snow particles in a core of ice and a shell of water. The model has a limited range of possibilities for accurate and validated results, meaning that the size and the ratio of the core and the shell are limited and cannot be out of a given range. Using a lognormal distribution generates very large and very small particles that are out of the range accessible to the layered code. To be consistent, we should have used the same distribution as in our previous publication, but that distribution should have been truncated in order to be in the range of validated particle sizes for the layered code. We therefore did not use any lognormal distribution in the layered code. Given the range of SSA values used here, the effect on calculated reflectance by the model is most likely insignificant. To allow meaningful comparisons, we did not use a lognormal distribution in the Mie code either. New polynomial fits were therefore determined for both codes, which are valid for snow grain sizes without a lognormal distribution.

Acknowledgements. F. Domine thanks CEN Grenoble for hosting him to carry out the experimental work. The assistance of François Touvier to operate the snow heater and of Jean-Michel Panel and Jacques Roulle to operate the cold room are gratefully acknowledged. J.-C. Gallet was supported through the projects "Long Range transport of Black Carbon and the effect on snow albedo in North East China and in the Arctic" funded by the Norwegian Research Council (Norklima program, project 193717) and "Satellite Remote Sensing of Atmosphere-Surface Systems and Ground Truth Measurements" funded by the Norwegian Research Council (Norklima program, project 209681/E10).

Edited by: M. Schneebeli

References

Aoki, T., Fukabori, M., Hachikubo, A., Tachibana, Y., and Nishio, F.: Effects of snow physical parameters on spectral albedo and bidirectional reflectance of snow surface, J. Geophys. Res.-Atmos., 105, 10219–10236, 2000.

Arnaud, L., Picard, G., Champollion, N., Domine, F., Gallet, J., Lefebvre, E., Fily, M., and Barnola, J. M.: Measurement of vertical profiles of snow specific surface area with a one centimeter resolution using infrared reflectance: Instrument description and validation, J. Glaciol., 57, 17–19, 2011.

Brun, E.: Investigation on wet-snow metamorphism in respect of liquid-water content, Ann. Glaciol., 13, 22–26, 1989.

Brun, E., David, P., Sudul, M., and Brunot, G.: A numerical-model to simulate snow-cover stratigraphy for operational avalanche forecasting, J. Glaciol., 38, 13–22, 1992.

Brzoska, J. B., Coleou, C., and Lesaffre, B.: Thin-sectioning of wet snow after flash-freezing, J. Glaciol., 44, 54–62, 1998.

Colbeck, S. C.: Theory of metamorphism of wet snow, United States Army Corps of Engineers, Hanover, NH, USACRREL Report 73, 1–11, 1973.

Colbeck, S. C.: An overview of seasonal snow metamorphism, Rev. Geophys., 20, 45–61, 1982.

Coleou, C. and Lesaffre, B.: Irreducible water saturation in snow: experimental results in a cold laboratory, in: Ann. Glaciol., Vol 26, 1998, edited by: McClung, D. M., Ann. Glaciol., 64-68, 1998.

Domine, F., Taillandier, A. S., and Simpson, W. R.: A parameterization of the specific surface area of seasonal snow for field use and for models of snowpack evolution, J. Geophys. Res.-Earth Surf., 112, F02031, doi:10.1029/2006jf000512, 2007.

Domine, F., Gallet, J. C., Barret, M., Houdier, S., Voisin, D., Douglas, T., Blum, J. D., Beine, H., and Anastasio, C.: The specific surface area and chemical composition of diamond dust near Barrow, Alaska, J. Geophys. Res., 116, D00R06, doi:10.1029/2011JD016162, 2011.

Dozier, J., and Painter, T. H.: Multispectral and hyperspectral remote sensing of alpine snow properties, Annual Review of Earth and Planetary Sciences, 32, 465–494, doi:10.1146/annurev.earth.32.101802.120404, 2004.

Erbe, E. F., Rango, A., Foster, J., Josberger, E. G., Pooley, C., and Wergin, W. P.: Collecting, shipping, storing, and imaging snow crystals and ice grains with low-temperature scanning electron mircoscopy, Microsc. Res. Tech., 62, 19–32, doi:10.1002/jemt.10383, 2003.

Fierz, C., Armstrong, R. L., Durand, Y., Etchevers, P., Greene, E., McClung, D. M., Nishimura, K., Satyawali, P. K., and Sokratov, S. A.: The International classification for seasonal snow on the ground UNESCO-IHP, ParisIACS Contribution No. 1, 80, 2009.

Flin, F., Brzoska, J. B., Lesaffre, B., Coleou, C. C., and Pieritz, R. A.: Three-dimensional geometric measurements of snow microstructural evolution under isothermal conditions, Ann. Glaciol., 38, 39–44, 2004.

Gallet, J.-C., Domine, F., Zender, C. S., and Picard, G.: Measurement of the specific surface area of snow using infrared reflectance in an integrating sphere at 1310 and 1550 nm, The Cryosphere, 3, 167–182, doi:10.5194/tc-3-167-2009, 2009.

Green, R. O., Dozier, J., Roberts, D., and Painter, T.: Spectral snow-reflectance models for grain-size and liquid-water fraction in melting snow for the solar-reflected spectrum, edited by: Winther, J. G., and Solberg, R., Ann. Glaciol., 34, 71–73, 2002.

Green, R. O., Painter, T. H., Roberts, D. A., and Dozier, J.: Measuring the expressed abundance of the three phases of water with an imaging spectrometer over melting snow, Water Resour. Res., 42, W10402, doi:10.1029/2005wr004509, 2006.

Hall, A.: The role of surface albedo feedback in climate, J. Climate, 17, 1550–1568, 2004.

Ketcham, W. M. and Hobbs, P. V.: An experimental determination of surface energies of ice, Phil. Mag., 19, 1161–1173, doi:10.1080/14786436908228641, 1969.

Legagneux, L., Cabanes, A., and Domine, F.: Measurement of the specific surface area of 176 snow samples using methane adsorption at 77 K, J. Geophys. Res.-Atmos., 107, 4335, doi:10.1029/2001jd001016, 2002.

Lemke, P., Ren, J., Alley, R. B., Allison, I., Carrasco, J., Flato, G., Fujii, Y., Kaser, G., Mote, P., Thomas, R. H., and Zhang, T.: Observations Changes in Snow, Ice and Frozen Ground, in: Climate Change 2007: The physical Sciences Basis, edited by: Pachauri, R. K., and Reisinger, A., IPCC, Geneva, Switzerland, 2007.

Matzl, M. and Schneebeli, M.: Measuring specific surface area of snow by near-infrared photography, J. Glaciol., 52, 558–564, 2006.

Montpetit, B., Royer, A., Langlois, A., Cliche, P., Roy, A., Champollion, N., Picard, G., Domine, F., and Obbard, R.: New shortwave infrared albedo measurements for snow specific surface area retrieval, J. Glaciol., 58, 941–952, doi:10.3189/2012JoG11J248, 2012.

Nolin, A. W. and Dozier, J.: A hyperspectral method for remotely sensing the grain size of snow, Remote Sens. Environ., 74, 207–216, doi:10.1016/s0034-4257(00)00111-5, 2000.

Painter, T. H., Molotch, N. P., Cassidy, M., Flanner, M., and Steffen, K.: Instruments and methods – Contact spectroscopy for determination of stratigraphy of snow optical grain size, J. Glaciol., 53, 121–127, 2007.

Picard, G., Arnaud, L., Domine, F., and Fily, M.: Determining snow specific surface area from near-infrared reflectance measurements: Numerical study of the influence of grain shape, Cold Reg. Sci. Technol., 56, 10–17, doi:10.1016/j.coldregions.2008.10.001, 2009.

Schaepman-Strub, G., Schaepman, M. E., Painter, T. H., Dangel, S., and Martonchik, J. V.: Reflectance quantities in optical remote sensing-definitions and case studies, Remote Sens. Environ., 103, 27–42, doi:10.1016/j.rse.2006.03.002, 2006.

Segelstein, D. J.: The complex refractive index of water, Master's, University of Missouri-Kansas City, 167 pp., 1981.

Stamnes, K., Tsay, S. C., Wiscombe, W., and Jayaweera, K.: Numerically stable algorithm for discrete-ordinate-method radiative-transfer in multiple-scattering and emitting layered media, Appl. Optics, 27, 2502–2509, 1988.

Taillandier, A. S., Domine, F., Simpson, W. R., Sturm, M., and Douglas, T. A.: Rate of decrease of the specific surface area of dry snow: Isothermal and temperature gradient conditions, J. Geophys. Res.-Earth Surf., 112, F03003, doi:10.1029/2006jf000514, 2007.

Toon, O. B. and Ackerman, T. P.: Algorithms for the calculation of scattering by stratified spheres, Appl. Optics, 20, 3657–3660, doi:10.1364/ao.20.003657, 1981.

Warren, S. G.: Optical-properties of snow, Rev. Geophys., 20, 67–89, 1982.

Warren, S. G. and Brandt, R. E.: Optical constants of ice from the ultraviolet to the microwave: A revised compilation, J. Geophys. Res.-Atmos., 113, D14220, doi:10.1029/2007jd009744, 2008.

Warren, S. G. and Wiscombe, W. J.: A model for the spectral albedo of snow .2. Snow containing atmospheric aerosols, J. Atmos. Sci., 37, 2734–2745, 1980.

Wergin, W. P., Rango, A., and Erbe, E. F.: Observations of snow crystals using low-temperature scanning electron microscopy, Scanning, 17, 41–50, doi:10.1002/sca.4950170106, 1995.

Wiscombe, W. J. and Warren, S. G.: A model for the spectral albedo of snow .1. Pure snow, J. Atmos. Sci., 37, 2712–2733, 1980.